Journal of Visualized Experiments

Detection of G Protein-coupled Receptor Expression in Mouse Vagal Afferent Neurons Using Multiplex In Situ Hybridization

--Manuscript Draft--

Article Type:	Invited Methods Article - JoVE Produced Video
Manuscript Number:	JoVE62945R1
Full Title:	Detection of G Protein-coupled Receptor Expression in Mouse Vagal Afferent Neurons Using Multiplex In Situ Hybridization
Corresponding Author:	Laurent Gautron UNITED STATES
Corresponding Author's Institution:	
Corresponding Author E-Mail:	Laurent.Gautron@utsouthwestern.edu
Order of Authors:	Johnson Bob-Manuel
	Laurent Gautron
Additional Information:	
Question	**Response**
Please specify the section of the submitted manuscript.	Neuroscience
Please indicate whether this article will be Standard Access or Open Access.	Standard Access ($1400)
Please indicate the **city, state/province, and country** where this article will be **filmed**. Please do not use abbreviations.	Dallas, TX, USA
Please confirm that you have read and agree to the terms and conditions of the author license agreement that applies below:	I agree to the Author License Agreement
Please provide any comments to the journal here.	
Please confirm that you have read and agree to the terms and conditions of the video release that applies below:	I agree to the Video Release

TITLE:

Detection of G Protein-coupled Receptor Expression in Mouse Vagal Afferent Neurons Using Multiplex *In Situ* Hybridization

AUTHORS AND AFFILIATIONS:

Johnson Bob-Manuel[1], Laurent Gautron[1]

Center for Hypothalamic Research and Department of Internal Medicine, UTSouthwestern Medical Center at Dallas, TX 75390, USA

Email address of co-author:

Johnson Bob-Manuel (Johnson.Bob-Manuel@UTsouthwestern.edu)

Corresponding author:

Laurent Gautron (Laurent.Gautron@UTSouthwestern.edu)

KEYWORDS:

Neuroanatomy, signaling, histology, transcription, transmembrane receptors, peripheral nervous system, dissection, confocal microscopy, fluorescence.

SUMMARY:

Multiplex *in situ* hybridization (ISH) was employed to simultaneously visualize the transcripts for two G protein-coupled receptors and one transcription factor in the entire vagal ganglionic complex of the adult mouse. This protocol could be used to generate accurate maps of the transcriptional profiles of vagal afferent neurons.

ABSTRACT:

This study describes a protocol for the multiplex *in situ* hybridization (ISH) of the mouse jugular-nodose ganglia, with a particular emphasis on detecting the expression of G protein-coupled receptors (GPCRs). Formalin-fixed jugular-nodose ganglia were processed with the RNAscope technology to simultaneously detect the expression of two representative GPCRs (cholecystokinin and ghrelin receptors) in combination with one marker gene of either nodose (paired-like homeobox 2b, Phox2b) or jugular afferent neurons (PR domain zinc finger protein 12, Prdm12). Labeled ganglia were imaged using confocal microscopy to determine the distribution and expression patterns of the aforementioned transcripts. Briefly, Phox2b afferent neurons were found to abundantly express the cholecystokinin receptor (Cck1r) but not the ghrelin receptor (Ghsr). A small subset of Prdm12 afferent neurons was also found to express Ghsr and/or Cck1r. Potential technical caveats in the design, processing, and interpretation of multiplex ISH are discussed. The approach described in this article may help scientists in generating accurate maps of the transcriptional profiles of vagal afferent neurons.

INTRODUCTION:

The cell bodies of vagal afferents are contained in the jugular, petrosal, and nodose ganglia[1-3]. Their axons travel together *via* several branches of the vagus nerve to craniocervical, thoracic,

and abdominal territories[4-7]. From their visceral endings, vagal afferents can respond to a wide range of physiological and noxious stimuli[8-10]. However, the distribution of signaling molecules and receptors involved in vagal sensing remains poorly characterized. This is partly because the vagal ganglia, in spite of their small size, express a broad spectrum of receptors, including a large number of GPCRs[8,11-13]. Moreover, vagal afferent neurons are inherently heterogeneous and display distinct molecular profiles[14]. To complicate the matter, the jugular, petrosal, and nodose ganglia are attached in the mouse, thereby forming a single ganglionic mass. Lastly, in a subset of animals, the nodose ganglion is attached to the sympathetic superior cervical ganglion[15].

In the past, investigators have turned to immunohistochemistry to study the neurochemical make-up of vagal afferent neurons[16-18]. While immunohistochemistry using validated antibodies is useful, the results of immunohistochemical studies must be interpreted with caution. For example, numerous efforts to identify specific antibodies against GPCRs have failed[19-25], leading investigators to conclude that the majority of antibodies against GPCRs are unreliable. To circumvent these issues, quantitative PCR (qPCR) has been widely used for assessing gene expression in the rodent vagal ganglionic mass[26-29]. However, examining gene expression using qPCR occurs at the cost of a loss of spatial information. In particular, it cannot be predicted how many cells or what cell type(s) express a particular gene of interest (e.g., nodose vs. jugular cells). Recurring issues also include the contamination with adjacent tissues and the inclusion of variable lengths of the vagus nerve, superior cervical, and jugular ganglia during dissection[15]. As a result of the above difficulties, controversy surrounds the expression and distribution of several GPCRs in vagal afferent neurons. One particularly puzzling example relates to the ghrelin receptor (Ghsr). Whereas some studies have found widespread expression of this receptor in vagal afferent neurons[30-32], others have found Ghsr mRNA to be nearly undetectable in the nodose ganglion[11,14]. Detailed mapping of Ghsr mRNA in the vagal ganglionic mass is therefore warranted.

In situ hybridization (ISH) has also been used to assess gene expression patterns in the vagal ganglionic mass[7,11,12,33-35]. Because RNA-based techniques remain more reliable and specific than antibody-based techniques under most circumstances[36,37], ISH studies have proven valuable for better understanding of the neurochemical coding of vagal afferent neurons. Nonetheless, traditional ISH techniques themselves are not without caveats. Radioactive ISH is sensitive but generates background and remains cumbersome[38]. Non-radioactive ISH is less complicated but also less sensitive[38]. In contrast, the recently developed RNAscope ISH method is highly sensitive and generates minimal background[39]. The current study applied multiplex fluorescent RNAscope to the detection of GPCRs in vagal afferent neurons of the mouse. We focused on mapping the distribution of Ghsr and compared its distribution to that of the cholecystokinin receptor (Cck1r), another GPCR well known to be expressed in the nodose ganglion[34]. Lastly, the two transcription factors, paired-like homeobox 2b (Phox2b) and PR domain zinc finger protein 12 (Prdm12), were used as selective markers for nodose and jugular afferent neurons, respectively[14]. Without visualizing Phox2b or Prdm12, it would be challenging to identify jugular vs. nodose afferents with certainty. Potential technical pitfalls are also discussed throughout the article.

PROTOCOL:

NOTE: Mice used in this study were wild-type males on a pure C57BL/6J background. A total of 4 mice were used for multiplex ISH. All mice were approximately 8 weeks old at the time of sacrifice. One male mouse (approximately one-year-old) was also used to demonstrate endogenous fluorescence associated with aging. Animals were housed in ventilated cages within a barrier facility with *ad libitum* access to food and water. The UT Southwestern Medical Center Institutional Animal Care and Use Committee reviewed and approved the procedures described below. Details about reagents and tools can be found in the **Table of Materials.**

1. Sample collection

1.1. On the day of sacrifice, administer an overdose of chloral hydrate (500 mg/kg, i.p.) to the mice. Perfuse the deeply anesthetized mice transcardially using a peristaltic pump with 5 mL of 1x phosphate-buffered saline (PBS) followed by 50 mL of 10% formalin at room temperature.

NOTE: This is done in a fume hood to prevent inhalation of formalin.

1.2. As the nodose, petrosal, and jugular ganglia are fused to form a single ganglionic mass in the mouse[15], carefully collect the entire vagal ganglionic mass from each side (left and right) with the help of a dissecting scope and fine spring scissors and forceps (see the **Table of Materials**).

1.3. When decapitating the mouse with a pair of large scissors (see the **Table of Materials**), avoid crushing the brainstem.

1.4. Following a dissection approach described before in the rat[40], remove the sternohyoid and omohyoid muscles lateral to the trachea with small forceps (**Table of Materials**) to expose the occipital bone. Clear the whole region of muscle, adipose tissue, and conjunctive tissue until the carotid artery, vagus nerve, the hypoglossal nerve, and foramen magnum are visible. Cut the entire hypoglossal nerve with small spring scissors (**Table of Materials**).

1.5. Look for the nodose ganglion as a translucent mass close to the foramen magnum[15]. Using small scissors (**Table of Materials**), carefully break the occipital bone to further expose the jugular ganglion. Look for black melanocytes at the surface of the jugular as a visual landmark.

1.6. Cut nerve attachments between the vagal ganglionic mass and extract the whole ganglionic mass by gently pulling on the peripheral end of the vagus nerve while simultaneously cutting the jugular ganglion towards the brainstem with small spring scissors (**Table of Materials**).

1.7. Remove the conjunctive tissue and fat sticking to the vagus nerve and ganglionic mass as much as possible.

1.8. As it is easy to lose one ganglion during the transfer from one tube to the other, keep ~0.5 cm of the vagus nerve to facilitate handling and localization of samples.

1.9. Place ganglia with the help of fine forceps in 1.5 mL microcentrifuge tubes and incubate at 4 °C in formalin for 24 h and with 30% sucrose for another 24 h.

1.10. Position ganglia inside a small drop (~4 mm Ø) of optimum cutting temperature (OCT) medium on a piece of aluminum foil. Next, freeze the sample on a bed of dry ice.

1.11. Cut the samples with a cryostat at -20 °C into sections of 14 µm thickness and collect on glass microscope slides as 3 series 42 µm apart.

NOTE: Avoid placing sections close to the edges of the slide. To save reagents, keep the tissue sections as tightly packed as possible but without overlapping.

1.12. Store the samples in a -80 °C freezer until needed for ISH for at least 6 months.

NOTE: Refer to **Figure 1** for troubleshooting for endogenous fluorescence.

2. Pretreatment and ISH

2.1. Before the day of the experiments, autoclave laboratory glassware to be used for ISH, including staining dishes and washing buffer jars.

NOTE: While working under RNase-free conditions is not critical, wear gloves at all times. Keep RNase decontamination solution bottles (**Table of Materials**) within reach in case contamination is suspected.

2.2. On the first day, bring the slides to room temperature on a bench specifically dedicated to ISH. Rinse the slides in 1x PBS and bake them for 30 mins at 60 °C in a baking oven (**Table of Materials**).

2.3. Post-fix the slides in 4% formalin for 15 min at 4 °C.

2.4. Bring the reagents in the multiplex kit (**Table of Materials**) to room temperature.

2.5. Dehydrate the slides in 50%, 70%, and 100% ethanol for 5 min each. Apply H_2O_2 solution to the samples for 10 min and then rinse in double-distilled water (ddH_2O).

2.6. Treat the samples with the target retrieval reagent for 5 min, rinse in ddH_2O followed by 100% ethanol, and air-dry. Using a hydrophobic pen, create a barrier around the samples.

NOTE: Do not apply the hydrophobic barrier too close to the tissue sections.

2.7. Apply protease for 30 min at 40 °C in a hybridization oven (**Table of Materials**).

2.8. In the meantime, prewarm the probes at 40 °C and cool them at room temperature before use. Incubate the slides with the desired combination of target probes (Cck1r-C3, Ghsr-C1, Phox2b-C2; or Cck1r-C3, Ghsr-C1, Prdm12-C2) for 2 h at 40 °C in a hybridization oven.

2.9. Incubate negative control tissue with the dihydrodipicolinate reductase (DapB) target C1 probe for 2 h at 40 °C in a hybridization oven.

2.10. Rinse the slides in wash buffer and store overnight in 5x saline sodium citrate (SSC) at room temperature. For convenience, split the experiment into two days. On the following day, rinse the slides with wash buffer and incubate them with amplification reagents listed below (see the user manual in **Table of Materials**).

2.11. Apply AMP1 (30 min at 40 °C), AMP2 (30 min at 40 °C), and AMP 3 (15 min at 40 °C). Rinse in wash buffer between each step.

2.12. Dissolve each Opal dye (**Table of Materials**) in dimethyl sulfoxide and store the solutions at 4 °C until needed.

2.13. For channel 1, incubate the slides with HRP-C1 (15 min at 40 °C) and Opal 520 (green color; dilution 1/1,500; 30 mins at 40°C). Rinse in wash buffer between each step.

2.14. For channel 2, incubate the slides with HRP-C2 (15 min at 40 °C) and Opal 570 (yellow color; dilution 1/1,500; for 30 min at 40 °C). Rinse in wash buffer between each step.

2.15. For channel 3, incubate the slides with HRP-C3 (15 min at 40 °C) and Opal 690 (far red color; dilution 1/1,500; for 30 min at 40 °C). Rinse in wash buffer between each step.

2.16. Wash the slides and expose them to 4',6-diamidino-2-phenylindole (DAPI) for 30 s.

2.17. Immediately apply mounting medium on each slide and place a coverslip over the tissue section.

2.18. Keep the tissues horizontal in a slide holder at 4 °C until imaging.

3. Microscopy and data analysis

NOTE: Multiplex ISH data can be imaged with a wide range of instruments with the appropriate filters. However, a preferred imaging method is confocal microscopy with 20x and 63x (oil) objectives; refer to the discussion for the reasons. Refer to **Figure 2** for the determination of the optimal signal-to-noise ratio.

3.1. Use a confocal microscope equipped with 488, 561, and 633 nm laser lines. Use the following acquisition parameters (see **Table 1**): Opal 690 (HeNe 633 nm, detection range 668–696 nm, power 2.0, gain 724); Opal 570 (DPSS laser 561 nm, detection range 579–627 nm, <power

15.0, <gain 450); Opal 520 (argon laser 488 nm, detection range 499–535 nm , <power 6.0, <gain 830); DAPI (diode laser 405, detection range 415–502 nm, <power 12.0, <gain 532).

3.2. To improve the quality of the images, acquire with a line averaging of 4 and a pixel size of at least 1024 x 1024.

NOTE: The above parameters are only provided as an example, and modifications are recommended depending on one instrument, magnification (20x or 63x), expression levels, and endogenous levels of fluorescence for any given tissue.

3.3. Once satisfied with the acquisition parameters, collect images using the same settings. Attribute false colors to each channel to facilitate visualization.

NOTE: For example, red (Phox2b or Prdm12), cyan (Cck1r), yellow (Ghsr), and grey (DAPI).

3.4. Perform cell counting using the digital images by identifying the outline of RNAscope-positive profiles with one nucleus lightly stained with DAPI. Calculate the percentage of RNAscope-positive profiles expressing each transcript [**Figure 3A–C**].

3.5. To improve the rigor and accuracy of the estimates, count at least 2,000 neuronal profiles from at least 4 different animals. Perform counting from left and right ganglia separately.

3.6. Input the data in a pie chart with the total number of counted profiles.

3.7. Use imaging software to acquire images and stitch together 20x images. Use ImageJ-Fiji and another photo and design software to generate the final plates. Apply adjustments to contrast and lightness uniformly to all images.

REPRESENTATIVE RESULTS:

While RNAScope can be applied to animals of any age, sex, or genetic background, it is advisable to work with young adults (<3 months old). This is because fluorescent artifacts (e.g., lipofuscin) are common findings in neurons of older animals[41]. The formalin-fixed ganglia from older mice often contain surprisingly intense endogenous fluorescence that can easily be mistaken for genuine staining (**Figure 1A,B**). In any case, it is advisable to verify the levels of endogenous fluorescence in the tissue before processing.

It is important to determine optimal acquisition parameters and signal-to-noise ratio for each laser and magnification using sections from a negative control tissue incubated with the DapB negative probe as shown in **Figure 2A,B**. Because *DapB* is a prokaryotic gene, RNAscope signals should be completely absent from the negative control tissue. Aside from occasional debris and crystals, negligible fluorescence is seen in images from negative control tissues, provided the acquisition parameters are used are appropriate. However, above a certain laser power and gain, unwanted background and random fluorescent dots start appearing (**Figure 2C**). Another purpose of minimizing laser power is to avoid pixel saturation and photobleaching. No major

issues of fluorescence bleaching were observed when working with the above parameters. If such an issue may arise, it is advisable to cover the tissue with a mounting medium for fluorescently labeled cells (**Table of Materials**) in addition to lowering the laser power as much as possible (see the recommended parameters in **Table 1**).

The RNAscope technique was applied for the detection of 3 genes in tissue sections of the vagal ganglionic mass of the mouse (**Figure 3** and **Figure 4**). One profile was considered positive for Ghsr and/or Cck1r when yellow and/or cyan dots, respectively, were seen overlaying one profile filled with red dots (**Figure 3A–C**). The example given in **Figure 3** shows many profiles containing both Phox2b and Cck1r transcripts (**Figure 3D**). Phox2b was used to identify nodose afferent neurons. Abundant Phox2b signals accumulated in the neurons of the nodose ganglion (**Figure 4A,B**). Cck1r signals were detected in approximately 52% of Phox2b cells (**Figure 4C**). Of note, expression levels for Cck1r greatly varied between cells, ranging from moderate (~20 dots per profile) to intense labeling (cytoplasm filled). In contrast, signals for Ghsr were extremely sparse in the nodose ganglion (**Figure 4A,B**). Only an estimated 0.65% of Phox2b-positive cells were also positive for Ghsr transcripts (**Figure 4C**). Ghsr-expressing cells often co-expressed Cck1r. A visual survey of the tissues did not reveal obvious differences between the left and right ganglia. ISH signals were virtually absent from areas devoid of neurons (e.g., epineurium and fiber tract).

Prdm12 was used to identify jugular afferent neurons. As expected, Prdm12 expression was highly enriched in the neurons of the jugular ganglion and a few neurons infiltrating the rostral portion of the nodose ganglion (**Figure 5A–C**). Interestingly, Cck1r signals were detected in a subset of Prdm12 cells (**Figure 5B,C**). Slightly less than 9% of Prdm12-positive neurons also expressed Cck1r (**Figure 5D**). However, the jugular ganglion only contains cells with moderate levels of Cck1r (<20 dots per cells) rather than the strongly labeled Cck1r-positive cells commonly found in the nodose ganglion. Ghsr-positive cells were significantly more prevalent in the jugular than in the nodose (**Figure 5C**). Approximately 3% of Prdm12 cells were also Ghsr-positive (**Figure 5D**). Interestingly, 1% of all Prdm12 co-expressed both Ghsr and Cck1r. Expression levels for Ghsr were always moderate (<20 dots per cell). No ISH signals could be seen in areas devoid of neurons.

FIGURE AND TABLE LEGENDS:

Figure 1: Troubleshooting issues of endogenous fluorescence. (**A, B**) Endogenous fluorescence in the nodose/jugular ganglion of one aging mouse (~1 year old). Digital images were acquired by confocal microscopy using the laser lines indicated in colors and acquisition parameters identical to those used for multiplex ISH with younger mice (see later). Importantly, the fixed tissue was not processed in any way other than being stored at -80 °C and exposed to DAPI. As shown in **A**, a significant level of unwanted fluorescence is observed in neuronal and non-neuronal cells, especially when exposed to the 488 nm laser (green). This is a common finding in histology, which warrants assessing endogenous fluorescence before histological analysis. (**B**) At higher magnification, fluorescence resembled lipofuscin pigments that often accumulate in aging cells and could easily be mistaken for genuine immunoreactivity and/or RNAScope signals. Scale bars = 158 µm (**A**) and 15 µm (**B**). (**B**). Abbreviations: DAPI = 4',6-diamidino-2-phenylindole; NG =

nodose ganglion; ISH = *in situ* hybridization.

Figure 2: Determining optimal signal-to-noise ratio. (**A, B**) Negative control consisting of RNAScope detection for the prokaryotic gene *DapB*. Note that endogenous fluorescence in the nodose ganglion of a young adult mouse is minimal, and that incubation with the DapB probe did not result in signals. Acquisition parameters were identical to those used for multiplex ISH. This shows that the RNAScope procedure itself does not produce any significant background if acquisition parameters are chosen carefully. (**C**) Digital images of the same tissue acquired at increasing power laser and gain with the 488 nm laser. Note how some fuzzy green background and occasional dots arise above a certain laser power and gain. Thus, it is important to carefully choose acquisition parameters for each laser based on the amount of unspecific fluorescence obtained in the negative control tissue. Scale bars = 158 µm (**A**) and 15 µm (**B, C**). Abbreviations: DapB = dihydrodipicolinate reductase; DAPI = 4',6-diamidino-2-phenylindole; NG = nodose ganglion; ISH = *in situ* hybridization.

Figure 3: Identification and counting of positive profiles. (**A**) Representative digital image of Phox2b-labeled profiles (red) in the rostral part of the nodose ganglion. In this example, a total of 18 cellular profiles (labeled as 1 to 18) were identified. Note that DAPI staining further helps in localizing neurons, which typically displayed a large and round nucleus with light DAPI stain. In contrast, the nuclei of non-neuronal cells are brightly labeled, elongated, and smaller in size. Overall, the RNAScope signals conformed to the distribution and shape of neuronal rather than non-neuronal cells. (**B**) Two labeled Ghsr-positive neurons (yellow) are shown (profiles 19 and 20). Ghsr signals were sparse and difficult to see. Therefore, the lightness and saturation of the yellow signals were selectively and uniformly enhanced in photo software. (**C**) A total of nine Cck1r-labeled profiles (cyan) are identified (labeled as 2, 5, 8, 11, 14, 17, 18, and 19). Note how the intensity of Cck1r signals varied greatly between cells. For example, profile 11 only contains a few positive signals, whereas profile 7 is almost filled with Cck1r signals. (**D**) A merged view of all channels allowed the identification of colocalization patterns. Many Phox2b-positive profiles also co-expressed Cck1r (e.g., profiles 2, 8, and 14), as evidenced by red and cyan RNAScope dots within the same cellular profile. In contrast, Phox2b-positive profiles did not express Ghsr transcripts (profiles 19 and 20). However, one Ghsr-positive cell also expressed low levels of Cck1r (profile 19). The two large DAPI-stained nuclei labeled with a white asterisk presumably correspond to the location of Phox2b-negative afferent neurons devoid of RNAScope signals. In the representative results described below, at least 2,000 neuronal profiles were counted from left and right ganglionic masses from 4 different animals. Scale bars = 24 µm. Abbreviations: DAPI = 4',6-diamidino-2-phenylindole; Phox2b = paired-like homeobox 2b; Ghsr = ghrelin receptor; Cck1r = cholecystokinin receptor.

Figure 4: Representative results of multiplex ISH in nodose afferent neurons. Digital images of a representative vagal ganglionic mass labeled with multiplex RNAscope for Phox2b, Cck1r, and Ghsr. Images were acquired with the 20x (**A**) and 63x (**B, C**) objectives of a confocal microscope (Zeiss LSM880). In **A**, 20× several images were stitched together using the Zen software and presented as either unmixed channels or merged. Phox2b signals (red) specifically accumulated in afferent neurons located in the nodose ganglion. As expected, Cck1r signals (cyan) intensely

labeled many, but not all, neurons in the nodose ganglion. At low magnification, cells expressing low levels of Cck1r or any cells with Ghsr signals (yellow) could not be observed easily. DAPI (gray) helped visualize the tissue and identify vagal afferent neurons with a large and lightly stained nucleus. The white inset in the merged image corresponds to the locations of the image included below. (**B**) At high magnification, Phox2b-positive profiles (red) are evident. Many cells also expressed Cck1r but at varying levels, ranging from moderate to very high. The profile "1" is an example of a Phox2b cell negative for Cck1r and Ghsr. Profiles "2" and "3" are Phox2b cells with high and moderate Cck1r signals, respectively. Moderate signals for Ghsr (yellow) were occasionally seen in the rostral nodose ganglion but almost always in cells negative for Phox2b, as shown with profile "4". Interestingly, profile "4" expressed both Ghsr and Cck1r. As shown in the next figure, Ghsr was more abundant in Prdm12 cells. (**C**) Pie chart summarizing the estimates of the percentage of Phox2b cells (red) co-expressing either Ghsr (yellow), Cck1r (cyan), or both (grey). The total number of counted profiles is indicated next to the chart (n=4 different ganglia, left and right combined). Results from each side were pooled because no differences were noticed. Scale bars = 158 µm (**A**) and 15 µm (**B**). Abbreviations: DAPI = 4',6-diamidino-2-phenylindole; NG = nodose ganglion; JG = jugular ganglion; ISH = *in situ* hybridization; Phox2b = paired-like homeobox 2b; Ghsr = ghrelin receptor; Cck1r = cholecystokinin receptor.

Figure 5: Representative results of jugular afferent neurons multiplex ISH. Digital images of a representative vagal ganglionic mass labeled with multiplex RNAscope Prdm12, Cck1r, and Ghsr. Images were acquired with the 20x (**A**) and 63x (**B, C**) objectives of a confocal microscope (Zeiss LSM880). In **A**, 20× several images were stitched together using the Zen software and presented as either unmixed channels or merged. Prdm12 transcript (red) specifically accumulated in afferent neurons located in the jugular ganglion and only a few neurons infiltrating the rostral part of the nodose ganglion. Cck1r signals (cyan) intensely labeled the nodose ganglion. At low magnification, cells expressing low levels of Cck1r or any cells with Ghsr signals (yellow) could not be seen easily. DAPI (gray) helped visualize the tissue and identify vagal afferent neurons with a large and lightly stained nucleus. The two white insets in the merged image correspond to the locations of the images included below. (**B, C**) At high magnification, Prdm12-positive cell profiles (red) can be delineated. Moderate signals for Cck1r were also detected in profiles "1" and "2". Profile "3" is representative of Prdm12 cells negative for Cck1r or Ghsr. In **C**, Ghsr signals (yellow) are seen in representative profile "4" but not in "5". (**D**) Pie chart summarizing the estimates of the percentage of Prdm12 cells (red) co-expressing either Ghsr (yellow), Cck1r (cyan), or both (grey). The total number of counted profiles is indicated next to the chart (n=4 different ganglia, left and right combined). Results from each side were pooled because no differences were noticed. Scale bars = 158 µm (**A**) and 15 µm (**B, C**). Abbreviations: DAPI = 4',6-diamidino-2-phenylindole; NG = nodose ganglion; JG = jugular ganglion; ISH = *in situ* hybridization; Prdm12 = PR domain zinc finger protein 12; Phox2b = paired-like homeobox 2b; Ghsr = ghrelin receptor; Cck1r = cholecystokinin receptor.

Table 1: Acquisition parameters. Abbreviation: DAPI = 4',6-diamidino-2-phenylindole.

DISCUSSION:

The technique of ISH was invented in the late 1960s[42]. However, it is not until the mid-1980s that it was applied for the detection of mRNAs in the central and peripheral nervous systems[43,44]. Considering the heterogeneity of the nervous system and recurring issues with antibodies, localizing a particular transcript at the cellular level remains an invaluable tool. Nonetheless, traditional ISH methods have remained laborious and variably sensitive. Fortunately, this study employed a highly sensitive ISH procedure called RNAscope, which usually generates no background and allows the detection of several transcripts expressed at low levels[45,46]. Specifically, multiplex fluorescent RNAScope was applied for the simultaneous detection of the Ghsr and Cck1r transcripts. The transcription factors, Phox2b and Prdm12, were further used as selective markers to differentiate nodose and jugular afferent neurons, respectively. Without visualizing Phox2b and Prdm12, it would be challenging to identify jugular vs. nodose afferent neurons with certainty. As explained above, one critical step includes a consistent and proper dissection technique. In addition, the verification of endogenous fluorescence is also an important factor as it could easily be mistaken for RNAScope signals. Furthermore, the choice of appropriate acquisition parameters based on negative control tissue is strongly advised. As mentioned earlier, confocal microscopy is the preferred imaging method with 20x and 63x (oil) objectives because 1) transcripts expressed at low levels and/or in sparse cells may only be noticeable at high magnification. 2) Confocal microscopy allows the collection of a single focal plane, which is important considering that two cells on top of each other may wrongly appear as one cell when imaged by epifluorescence. 3) Confocal microscopy also allows more selective and flexible acquisition parameters. The above acquisition parameters are only provided as an example, and modifications are recommended depending on one instrument, magnification (20x or 63x), expression levels, and endogenous levels of fluorescence for any given tissue. The staining procedure itself remained very close to that of the recommended protocol with only slight adjustments. Obviously, the protocol described here may be applied to the detection of any transcripts, not just GPCRs. The procedure described here is nonetheless particularly useful considering the recurring issues with antibodies raised against GPCRs[24].

As previously discussed[15], the mouse nodose ganglion is sometimes attached to the superior cervical ganglion by a cell bridge. The inclusion of this cell bridge may lead to confusing results, e.g., non-vagal markers being detected in the nodose ganglion. The investigator may want to systematically verify whether the nodose ganglion is attached to the superior cervical ganglion during dissection. Otherwise, inconsistent dissection skills between ganglia will introduce experimental variability. It is also important to note that both petrosal and nodose afferent neurons express Phox2b[47]. Thus, what we referred to as nodose afferent neurons included both petrosal and nodose neurons. Lastly, when comparing different studies, one should keep in mind that different methods of euthanasia can cause changes in gene expression[48].

In theory, the fluorophores used for detection can be interchangeably attributed to any channel. However, Opal 690 was found to emit a low level of green fluorescence. Under most circumstances, in the case of highly expressed transcripts (e.g., Prdm12), unwanted green fluorescence was seen if the laser intensity was too high. Opal 690 is therefore recommended for genes with moderate/low expression. If only working with highly expressed genes, it is recommended to dilute Opal 690 further (i.e., 1/3,000) and not capture unspecific green

fluorescence during image acquisition. RNAscope signals are separate dots of different colors, even when transcripts are expressed within the same cell profile. However, for highly expressed transcripts, it might not be possible to see individual dots but rather fluorescence filling up the cytoplasm. When dots emit fluorescence of different colors, one might consider a problem of unspecific fluorescence due to, among other examples, inadequate acquisition parameters and/or endogenous pigments. Lastly, Opal 570 and 620 must not be used simultaneously because their emission spectra overlap.

If no RNAscope signals are observed for a gene known to be expressed in the tissue of interest, it is advised to verify the integrity of the tissue by running a positive probe available (i.e., peptidyl-prolyl cis-trans isomerase B housekeeping gene). DAPI counterstaining is also helpful in determining tissue quality. DAPI-labeled nuclei that appear shredded may indicate excessive digestion or improperly fixed tissue.

As a result, Ghsr was expressed in a small subset of Prdm12-positive jugular afferent neurons. In contrast, and in agreement with one previous study[11], *Ghsr* mRNA was virtually absent from nodose afferent neurons. It is deduced that low levels of *Ghsr* mRNA previously detected by qPCR and ISH were likely due to jugular afferent neurons[30-32]. One prior calcium signaling study showed that 3% of cultured vagal afferent neurons respond to ghrelin[49], a number that is remarkably similar to the percentage of Ghsr-expressing jugular afferent neurons. Cck1r was expressed in many Phox2b-positive nodose afferent neurons and, more surprisingly, in a subset of Prdm12-positive jugular afferent neurons. In summary, this paper demonstrates the successful adaptation of existing ISH techniques to assess the cellular distribution of select GPCRs in the jugular-nodose ganglionic mass in its entirety.

In conclusion, multiplex ISH was employed to detect and simultaneously visualize the transcripts for two GPCRs (Cck1r and Ghsr) and one transcription factor (Phox2b or Prdm12) in the entire vagal ganglionic complex of the adult mouse. The protocol described here can be a complementary tool to RNA-Sequencing, qPCR, and traditional histology. However, this protocol may be applied to other ganglia of similar size. As discussed above, acquisition parameters, age of animals, and consistency of dissection are important factors to consider during experimental design. Therefore, it can offer unique information about the topographic gene expression patterns in a highly heterogeneous and small ganglion. This protocol could be used to determine changes in the transcriptional profiles of jugular vs. nodose afferent neurons in the context of various physiological and pathophysiological conditions, including, but not limited to, changes in feeding status. It may also be used to compare the neurochemical make-up of vagal afferent neurons in animal species commonly used in preclinical research, including primates and pigs[50,51].

ACKNOWLEDGMENTS:

This work was supported by the Neuroanatomy/Histology/Brain Injection Core funded by NIH grant #5P01DK119130-02. The authors would like to acknowledge the assistance of the UT Southwestern Live Cell Imaging Facility (headed by Dr. Phelps) and its staff (Abhijit Bugde and Marcel Mettlen), supported in part by the NIH Grant #1S10OD021684-01, a Shared Resource of the Harold C. Simmons Cancer Center, supported in part by an NCI Cancer Center Support Grant,

P30 CA142543.

DISCLOSURES:

The authors declare no competing financial interests.

REFERENCES:

1 Berthoud, H. R., Neuhuber, W. L. Functional and chemical anatomy of the afferent vagal system. *Autonomic Neuroscience.* **85** (1–3), 1–17 (2000).

2 Kim, S. H. et al. Mapping of sensory nerve subsets within the vagal ganglia and the brainstem using reporter mice for Pirt, TRPV1, 5-HT3, and Tac1 expression. *eNeuro.* **7** (2), ENEURO.0494-19.2020 (2020).

3 Atsumi, K. et al. Sensory neurons in the human jugular ganglion. *Tissue and Cell.* **64**, 101344 (2020).

4 Mazzone, S. B., Undem, B. J. Vagal afferent innervation of the airways in health and disease. *Physiological Reviews.* **96** (3), 975–1024 (2016).

5 Wang, F. B., Powley, T. L. Topographic inventories of vagal afferents in gastrointestinal muscle. *Journal of Comparative Neurology.* **421** (3), 302–324 (2000).

6 Prechtl, J. C., Powley, T. L. The fiber composition of the abdominal vagus of the rat. *Anatomy and Embryology.* **181** (2), 101–115 (1990).

7 Gautron, L. et al. Melanocortin-4 receptor expression in a vago-vagal circuitry involved in postprandial functions. *Journal of Comparative Neurology.* **518** (1), 6–24 (2010).

8 Williams, E. K. et al. Sensory neurons that detect stretch and nutrients in the digestive system. *Cell.* **166** (1), 209–221 (2016).

9 Chuaychoo, B., Hunter, D. D., Myers, A. C., Kollarik, M., Undem, B. J. Allergen-induced substance P synthesis in large-diameter sensory neurons innervating the lungs. *Journal of Allergy and Clinical Immunology.* **116** (2), 325–331 (2005).

10 Page, A. J., O'Donnell, T. A., Blackshaw, L. A. Opioid modulation of ferret vagal afferent mechanosensitivity. *American Journal of Physiology and Gastrointestinal Liver Physiology.* **294** (4), G963–970 (2008).

11 Egerod, K. L. et al. Profiling of G protein-coupled receptors in vagal afferents reveals novel gut-to-brain sensing mechanisms. *Molecular Metabolism.* **12**, 62–75 (2018).

12 Wang, J. et al. Distinct and common expression of receptors for inflammatory mediators in vagal nodose versus jugular capsaicin-sensitive/TRPV1-positive neurons detected by low input RNA sequencing. *PLoS One.* **12** (10), e0185985 (2017).

13 Bai, L. et al. Genetic identification of vagal sensory neurons that control feeding. *Cell.* **179** (5), 1129–1143 e23 (2019).

14 Kupari, J., Haring, M., Agirre, E., Castelo-Branco, G., Ernfors, P. An atlas of vagal sensory neurons and their molecular specialization. *Cell Reports.* **27** (8), 2508–2523 e2504 (2019).

15 Bookout, A. L., Gautron, L. Characterization of a cell bridge variant connecting the nodose and superior cervical ganglia in the mouse: Prevalence, anatomical features, and practical implications. *Journal of Comparative Neurology.* **529** (1), 111–128 (2021).

16 Gautron, L., Lee, C. E., Lee, S., Elmquist, J. K. Melanocortin-4 receptor expression in different classes of spinal and vagal primary afferent neurons in the mouse. *Journal of Comparative Neurology.* **520** (17), 3933–3948 (2012).

17 Broberger, C., Holmberg, K., Kuhar, M. J., Hokfelt, T. Cocaine- and amphetamine-regulated transcript in the rat vagus nerve: A putative mediator of cholecystokinin-induced satiety. *Proceedings of the National Academy of Sciences of the United States of America.* **96** (23), 13506–13511 (1999).
18 Yamamoto, Y., Henrich, M., Snipes, R. L., Kummer, W. Altered production of nitric oxide and reactive oxygen species in rat nodose ganglion neurons during acute hypoxia. *Brain Research.* **961** (1), 1–9 (2003).
19 Grimsey, N. L. et al. Specific detection of CB1 receptors; cannabinoid CB1 receptor antibodies are not all created equal! *Journal of Neuroscience Methods.* **171** (1), 78–86 (2008).
20 Morozov, Y. M. et al. Antibodies to cannabinoid type 1 receptor co-react with stomatin-like protein 2 in mouse brain mitochondria. *European Journal of Neuroscience.* **38** (3), 2341–2348 (2013).
21 Jelsing, J., Larsen, P. J., Vrang, N. Identification of cannabinoid type 1 receptor expressing cocaine amphetamine-regulated transcript neurons in the rat hypothalamus and brainstem using in situ hybridization and immunohistochemistry. *Neuroscience.* **154** (2), 641–652 (2008).
22 Jensen, B. C., Swigart, P. M., Simpson, P. C. Ten commercial antibodies for alpha-1-adrenergic receptor subtypes are nonspecific. *Naunyn-Schmiedeberg's Archives of Pharmacology.* **379** (4), 409–412 (2009).
23 Hamdani, N., van der Velden, J. Lack of specificity of antibodies directed against human beta-adrenergic receptors. *Naunyn-Schmiedeberg's Archives of Pharmacology.* **379** (4), 403–407 (2009).
24 Michel, M. C., Wieland, T., Tsujimoto, G. How reliable are G-protein-coupled receptor antibodies? *Naunyn-Schmiedeberg's Archives of Pharmacology.* **379** (4), 385–388 (2009).
25 Goodman, S. L. The antibody horror show: an introductory guide for the perplexed. *Nature Biotechnology.* **45**, 9–13 (2018).
26 Liu, C. et al. PPARgamma in vagal neurons regulates high-fat diet induced thermogenesis. *Cell Metabolism.* **19** (4), 722–730 (2014).
27 Zeeni, N. et al. A positive change in energy balance modulates TrkB expression in the hypothalamus and nodose ganglia of rats. *Brain Research.* **1289**, 49–55 (2009).
28 Kentish, S. J., Frisby, C. L., Kennaway, D. J., Wittert, G. A., Page, A. J. Circadian variation in gastric vagal afferent mechanosensitivity. *Journal of Neuroscience.* **33** (49), 19238–19242 (2013).
29 Peiser, C. et al. Dopamine D2 receptor mRNA expression is increased in the jugular-nodose ganglia of rats with nitrogen dioxide-induced chronic bronchitis. *Neuroscience Letters.* **465** (2), 143–146 (2009).
30 Date, Y. et al. The role of the gastric afferent vagal nerve in ghrelin-induced feeding and growth hormone secretion in rats. *Gastroenterology.* **123** (4), 1120–1128 (2002).
31 Meleine, M. et al. Ghrelin inhibits autonomic response to gastric distension in rats by acting on vagal pathway. *Scientific Reports.* **10** (1), 9986 (2020).
32 Zhang, W. et al. Functional interaction between Ghrelin and GLP-1 regulates feeding through the vagal afferent system. *Scientific Reports.* **10** (1), 18415 (2020).
33 Chang, R. B., Strochlic, D. E., Williams, E. K., Umans, B. D., Liberles, S. D. Vagal sensory neuron subtypes that differentially control breathing. *Cell.* **161** (3), 622–633 (2015).
34 Broberger, C., Holmberg, K., Shi, T. J., Dockray, G., Hokfelt, T. Expression and regulation of cholecystokinin and cholecystokinin receptors in rat nodose and dorsal root ganglia. *Brain*

573 *Research.* **903** (1–2), 128–140 (2001).
574 35 Hondoh, A. et al. Distinct expression of cold receptors (TRPM8 and TRPA1) in the rat
575 nodose-petrosal ganglion complex. *Brain Research.* **1319**, 60–69 (2010).
576 36 Hankin, R. C. In situ hybridization: principles and applications. *Laboratory Medicine.* **23**
577 764–770 (1992).
578 37 Baker, M. Reproducibility crisis: Blame it on the antibodies. *Nature.* **521** (7552), 274–276
579 (2015).
580 38 Dagerlind, A., Friberg, K., Bean, A. J., Hokfelt, T. Sensitive mRNA detection using unfixed
581 tissue: combined radioactive and non-radioactive in situ hybridization histochemistry.
582 *Histochemistry.* **98** (1), 39–49 (1992).
583 39 Wang, F. et al. RNAscope: a novel in situ RNA analysis platform for formalin-fixed,
584 paraffin-embedded tissues. *Journal of Molecular Diagnostic.* **14** (1), 22–29 (2012).
585 40 Norgren, R., Smith, G. P. A method for selective section of vagal afferent or efferent axons
586 in the rat. *American Journal of Physiology.* **267** (4 Pt 2), R1136–1141 (1994).
587 41 Schnell, S. A., Staines, W. A., Wessendorf, M. W. Reduction of lipofuscin-like
588 autofluorescence in fluorescently labeled tissue. *Journal of Histochemistry and Cytochemistry.* **47**
589 (6), 719–730 (1999).
590 42 Pardue, M. L., Gall, J. G. Molecular hybridization of radioactive DNA to the DNA of
591 cytological preparations. *Proceedings of the National Academy of Sciences of the United States*
592 *of America.* **64** (2), 600–604 (1969).
593 43 Villar, M. J. et al. Upregulation of nitric oxide synthase and galanin message-associated
594 peptide in hypothalamic magnocellular neurons after hypophysectomy. Immunohistochemical
595 and in situ hybridization studies. *Brain Research.* **650** (2), 219–228 (1994).
596 44 McAllister, L. B., Scheller, R. H., Kandel, E. R., Axel, R. In situ hybridization to study the
597 origin and fate of identified neurons. *Science.* **222** (4625), 800–808 (1983).
598 45 Bingham, V. et al. RNAscope in situ hybridization confirms mRNA integrity in formalin-
599 fixed, paraffin-embedded cancer tissue samples. *Oncotarget.* **8** (55), 93392–93403 (2017).
600 46 Kersigo, J. et al. A RNAscope whole mount approach that can be combined with
601 immunofluorescence to quantify differential distribution of mRNA. *Cell and Tissue Research.* **374**
602 (2), 251–262 (2018).
603 47 D'Autreaux, F., Coppola, E., Hirsch, M. R., Birchmeier, C., Brunet, J. F. Homeoprotein
604 Phox2b commands a somatic-to-visceral switch in cranial sensory pathways. *Proceedings of the*
605 *National Academy of Sciences of the United States of America.* **108** (50), 20018–20023 (2011).
606 48 Staib-Lasarzik, I. et al. Anesthesia for euthanasia influences mRNA expression in healthy
607 mice and after traumatic brain injury. *Journal of Neurotrauma.* **31** (19), 1664–1671 (2014).
608 49 Avau, B. et al. Ghrelin is involved in the paracrine communication between neurons and
609 glial cells. *Neurogastroenterology and Motility.* **25** (9), e599–608 (2013).
610 50 Settell, M. L. et al. Functional vagotopy in the cervical vagus nerve of the domestic pig:
611 implications for the study of vagus nerve stimulation. *Journal of Neural Engineering.* **17** (2),
612 026022 (2020).
613 51 Nyborg, N. C. B. et al. Cholecystokinin-1 receptor agonist induced pathological findings in
614 the exocrine pancreas of non-human primates. *Toxicology and Applied Pharmacology.* **399**,
615 115035 (2020).
616

Figure 1

Click here to access/download;Figure;Figure 1.tif

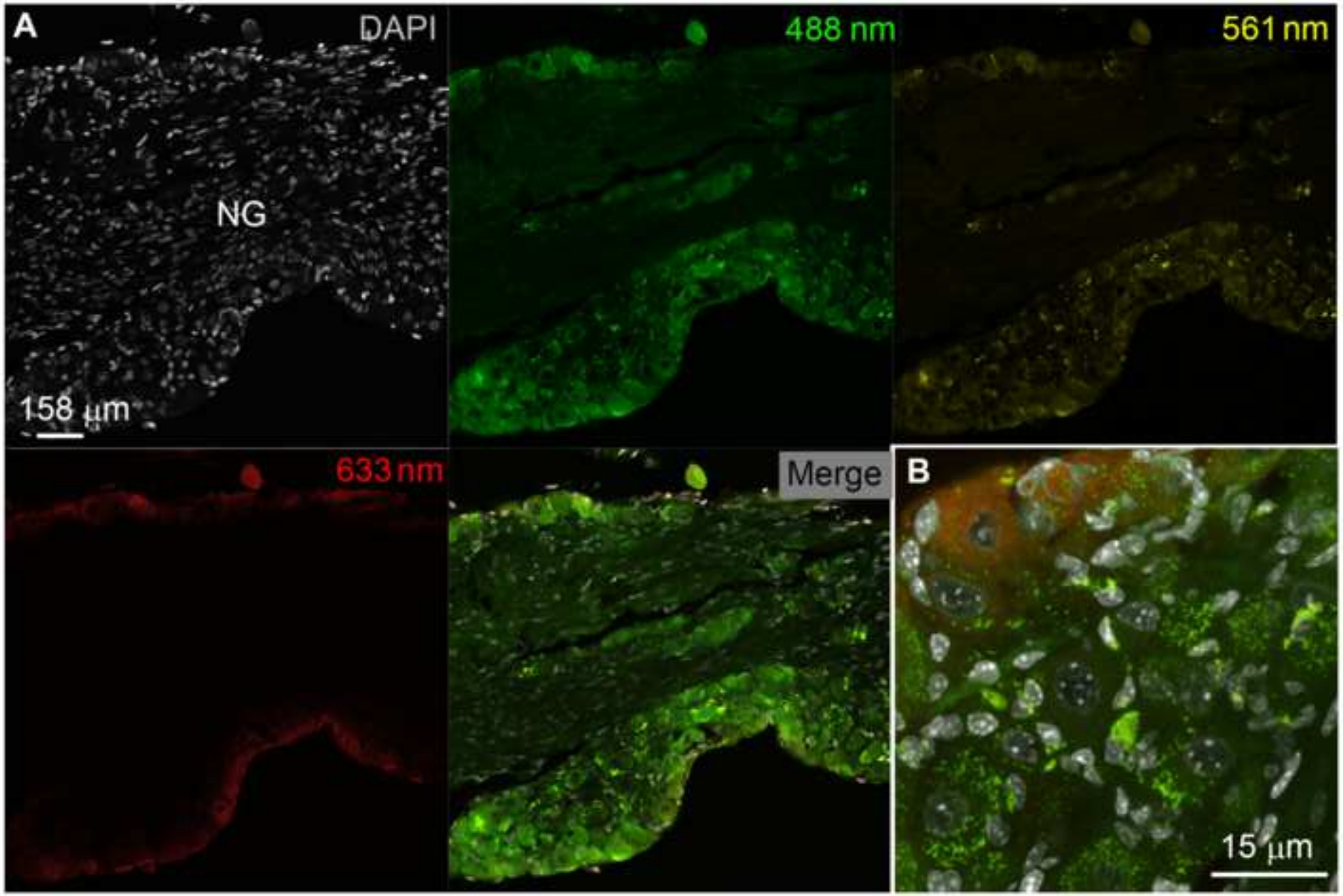

Figure 2

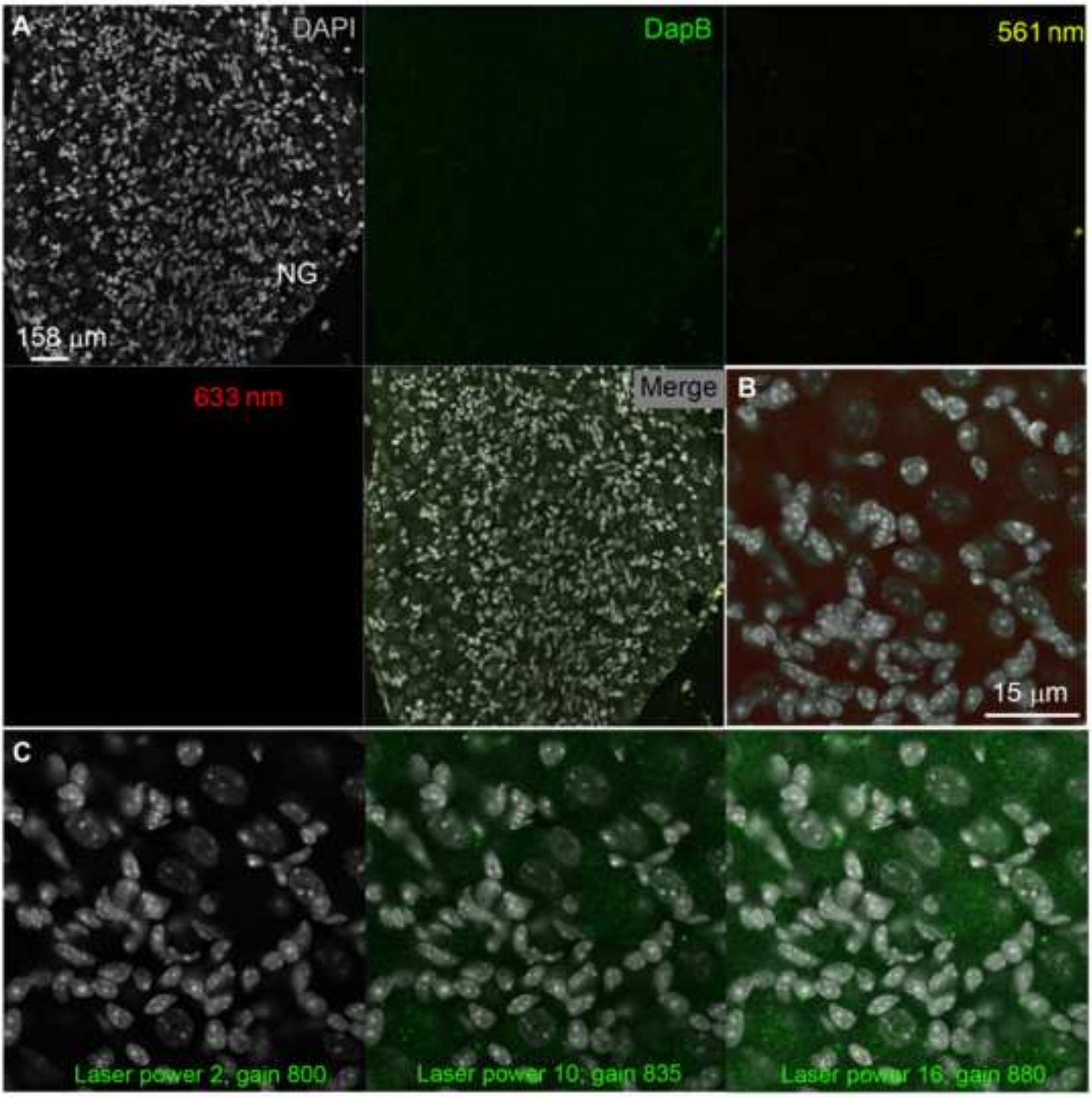

Figure 3

Click here to access/download;Figure;Figure 3.tif

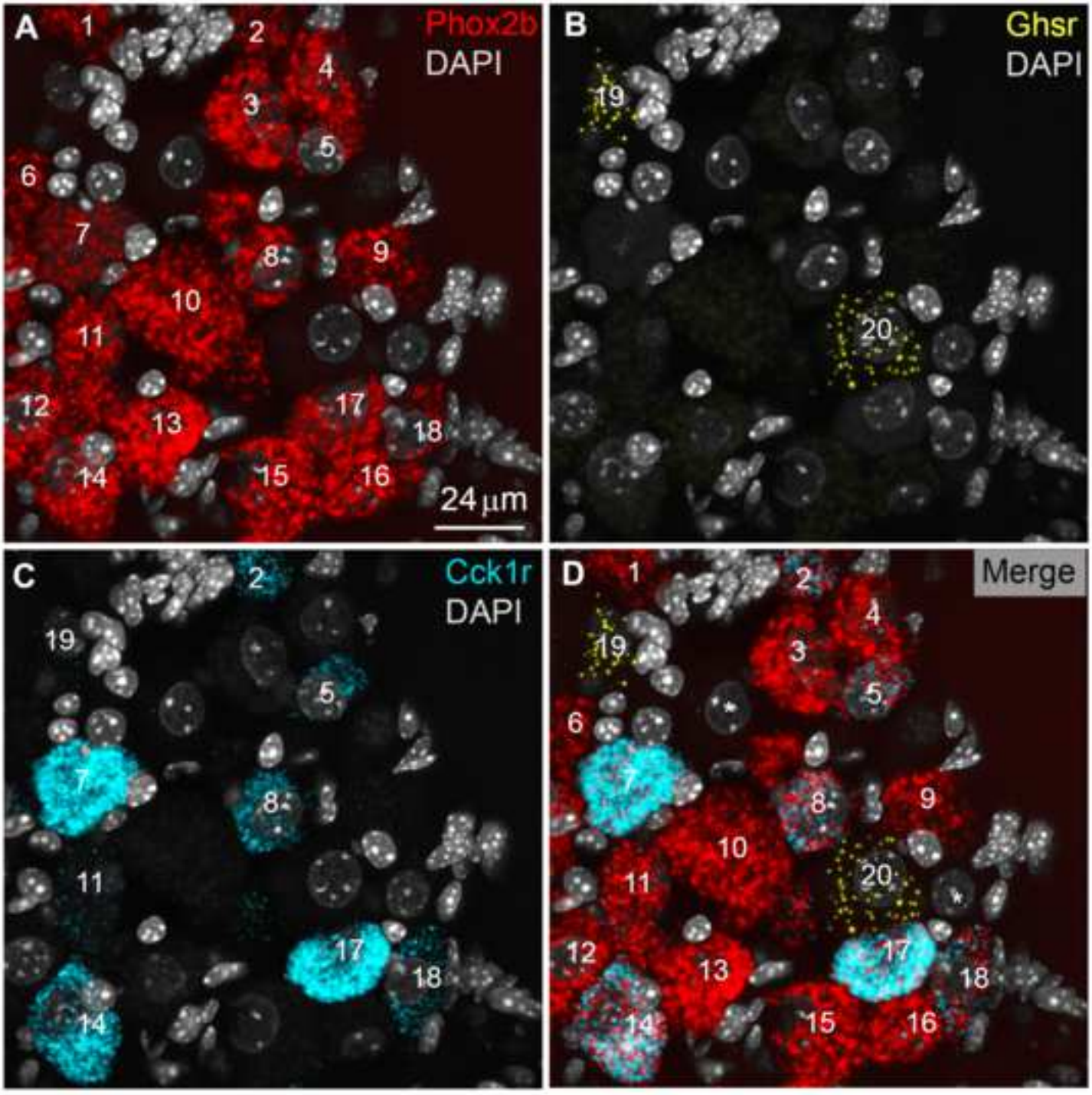

Figure 4

Click here to access/download;Figure;Figure 4.tif

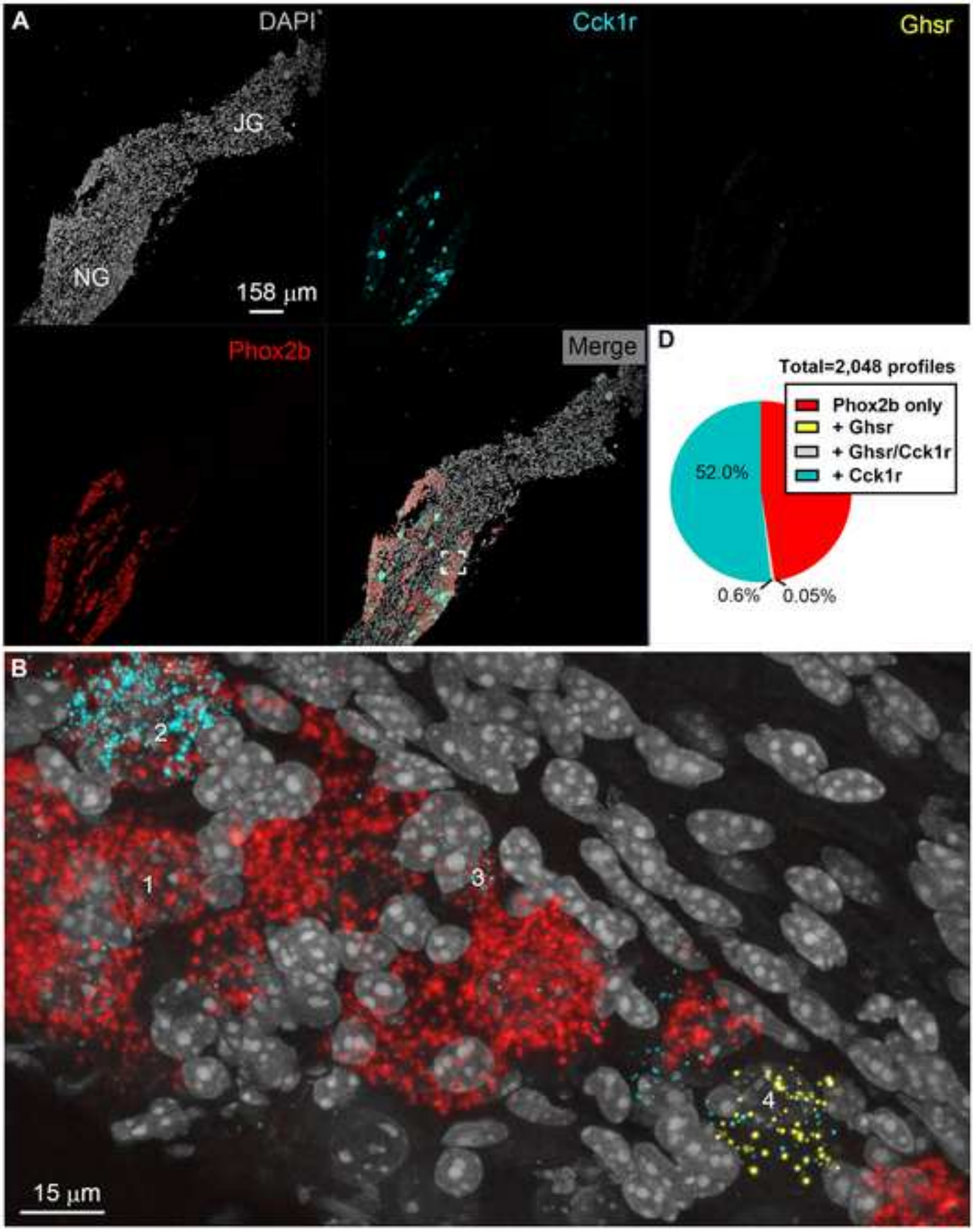

Figure 5

Click here to access/download;Figure;Figure 5.tif

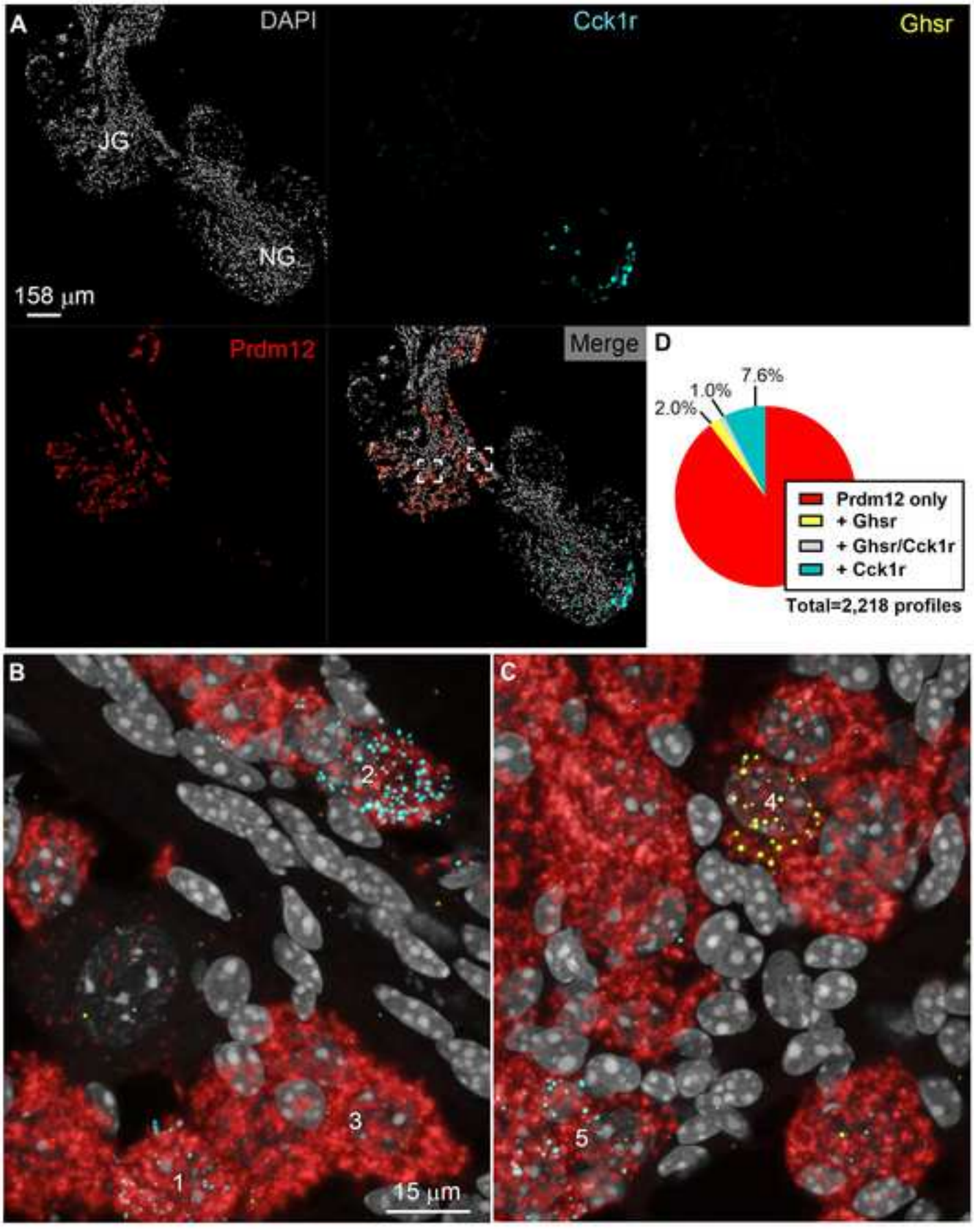

Table 1

Click here to access/download;Table;Table of acquisition parameters (1).xlsx

Opal	Laser line	Detection range	power	gain	Line average	Pixel size
Opal 690	HeNe 633 nm	668-696 nm	2	724	4	1024 x 1024
Opal 570	DPSS laser 561 nm	579-627 nm	15	450	4	1024 x 1024
Opal 520	argon laser 488 nm	499-535 nm	6	830	4	1024 x 1024
DAPI	diode laser 405	415-502 nm	12	532	4	1024 x 1024

Editorial comments:

Changes to be made by the Author(s):

1. Please take this opportunity to thoroughly proofread the manuscript to ensure that there are no spelling or grammar issues. We searched for spelling and grammar issues and corrected the text when necessary.

2. Please revise the text to avoid the use of any personal pronouns (e.g., "we", "you", "our" etc.). We revised the text (red highlight) to avoid using “we”, “you”, and “our”.

3. Please ensure that abbreviations are defined at first usage. Agree.

4. JoVE cannot publish manuscripts containing commercial language. This includes trademark symbols (™), registered symbols (®), and company names before an instrument or reagent. Please remove all commercial language from your manuscript and use generic terms instead. All commercial products should be sufficiently referenced in the Table of Materials. Please sort the Materials Table alphabetically by the name of the material. We removed the ® symbol following RNASCope.

5. The Protocol should be made up almost entirely of discrete steps without large paragraphs of text between sections. Please simplify the Protocol so that individual steps contain only 2-3 actions per step and a maximum of 4 sentences per step. We modified the structure of our protocol accordingly and included more steps.

6. Please ensure that all text in the protocol section is written in the imperative tense as if telling someone how to do the technique (e.g., “Do this,” “Ensure that,” etc.). The actions should be described in the imperative tense in complete sentences wherever possible. Avoid usage of phrases such as “could be,” “should be,” and “would be” throughout the Protocol. Any text that cannot be written in the imperative tense may be added as a “Note.” However, notes should be concise and used sparingly. We rewrote the protocol in the imperative tense.

7. Please note that your protocol will be used to generate the script for the video and must contain everything that you would like shown in the video. Please ensure you answer the “how” question, i.e., how is the step performed? Alternatively, add references to published material specifying how to perform the protocol action. There should be enough detail in each step to supplement the actions seen in the video so that viewers can easily replicate the protocol.

8. Please add more details to your protocol steps:

Step 1.1: Please mention whether the mentioned morning time is essential or not. Kindly note that anaesthetization steps cannot be filmed, so highlighting needs to be removed. Time is not essential and was removed. Step 1.1 is not highlighted anymore.

Step 1.2: Please specify what is meant by big scissor/small forcep? Any specific size is critical? The reference for scissors and forceps is now linked to the Table of Materials.

Line 118: How much the nerve should be cut? The entire hypoglossal nerve can be removed.

Line 129: Replace “Eppendorf” tube with “microcentrifuge” tube. Correction was made.

Line 137: How long the sample can be stored? At least 6 months.

Line 163: How the H2O2 treatment was performed? We added experimental details.

Line 172: Please mention the probes. The details can be given in the Table of Materials. Probes were added.

Line 205-206: Please mention the laser power used. Recommended power laser is listed in step 3.3. and new Table.

Step 3.3: Please provide a Table to list all the acquisition parameters. We created a new Table.

9. Please remove the phrase “Manufacturer’s instructions/protocols.”Instead, use generic terms. We removed the term “manufacturer”.

10. Please include a one-line space between each protocol step and then highlight up to 3 pages of the Protocol (including headings and spacing) that identifies the essential steps of the protocol for the video, i.e., the steps that should be visualized to tell the most cohesive story of the Protocol. Remember that non-highlighted Protocol steps will remain in the manuscript, and therefore will still be available to the reader. We modified the protocol accordingly.

11. Please modify the Result section to include all the observations and conclusions you can derive from the Figures. We reorganized the text to avoid including results in the Methods section.

12. Please ensure that scale bars are present in all the microscopic images. We think that all the needed scale bars are included.

13. Please spell out the journal titles in the References. References were corrected accordingly.

Reviewers' comments:

Reviewer #1:

Manuscript Summary:

The methods article entitled "Detection of G-proteins -coupled receptors expression in the mouse vagal afferents using multiplex in situ hybridization" by Bob-Manuel et. al describe a protocol that can be used for the visualization of vagal afferent neurons. To this end, the authors employ use of multiplex in situ hybridization (ISH) in the jugular and nodose ganglia of mice (marked by Prdm12 and Phox2b, respectively) and demonstrate the expression of cholecystokinin and ghrelin G-protein-coupled receptors (GPCRs). This manuscript serves as a valuable tool that will allow for greater understanding of vagal afferent transcriptional profile mapping. However, several minor weaknesses were found. Notably, there were grammatical and spelling errors throughout the document (including the title). There is also a need for greater experimental methodological detail. Otherwise, this is an interesting paper that could influence the neuroanatomical field.

We thank the reviewer for the comments. We apologize for the spelling errors.

Specific comments

1. In lines 79-80 the authors state "Phox2b and Prdm12 were further used as selective markers for jugular and nodose afferents, respectively". It's vice versa-please correct. We apologize for the mistake.

2. As we know feeding status influences expression of genes within the CNS, there should be discussion of how feeding status might influence the findings presented here and how to best control for feeding status for studies like these. We agree. One sentence was added on feeding status.

3. Similarly, do the authors have any idea whether the specific method of euthanasia will cause differences in expression patterns of vagal subtypes? This should also be discussed. This is a good point that we had not considered in the past. The article now discusses the possible effect of euthanasia on gene expression.

4. In lines 171-172, the authors mention that slides were "incubated with the combination of probes listed below for 2 hours at 40C (HybEZ oven)". Immediately after, the authors state "On the next morning" in lines 175 and 176. Is there an overnight incubation? If not, is a step missing here? We apologize for the confusion. Tissue is incubated with probes for 2 hours only. It is kept overnight in SSC buffer.

5. In section 3.3 of "Microscopy and data analysis", the authors provide a very thorough and precise description of their microscope parameters. While this is great for establishing a baseline for this specific confocal scope, it may not be as beneficial for readers with different brands of confocal microscopes. We agree. This is why we wrote that the above parameters are only provided as an example and modifications are recommended depending on one instrument, magnification (20x or 63x), and expression levels, endogenous levels of fluorescence for any given tissue.

6. The authors should also provide additional commentary on whether the vagal subtype compositions vary between the right and left nodose as it's been demonstrated that the function is drastically different. As mentioned in the article, a visual survey of the tissues did not reveal obvious differences between the left and right ganglia. To the best of our knowledge, the molecular make-up of vagal afferents located in the right vs left nodose is similar. Thus, the functional differences mentioned by the reviewer are likely due to differences in network connectivity.

7. There were grammatical and spelling errors throughout the document-including the title. It should be "Detection of G-protein-coupled receptor expression in the mouse vagal afferents….." We apologize for the mistake and corrected the article.

8. Section 2.3 of the "Pretreatment and Ish" section, the authors discuss use of Opal 520, 570, and 690 without giving a description as to what these reagents are/do. This is a good point. We added the missing information.

Reviewer #2:

Manuscript Summary:

The manuscript is clearly written and presents a well reasoned approach to the detection of GPCRs in mouse neuronal ganglia. Video documentation of the technique will be a useful addition to the primary

science literature. There are no major questions that need to be addressed or revisions that are required. Minor comments to improve the presentation are given below.

Minor Concerns:

Page 1: Suggest that the Ghsr and Cck1r acronyms be spelled out completely when first introduced and referred to only afterward by the respective acronyms. We agree. The proposed changes are included in the revised text.

Page 2: At line 53, the word, "letting" appears to be a typo that is better replaced with the word, "leading". We agree. The proposed changes are included in the revised text.

Page 5: At line 132, what is "OCT medium"? OCT stands for optimum cutting temperature.

Lastly, it may be helpful to the uninitiated reader to explain in a sentence or two, the rationale for using the DapB probe as a negative control. We agree. The revised text now explains what is dihydrodipicolinate reductase (DapB) and its relevance as a negative control.

Reviewer #3:

Manuscript Summary:

This manuscript describes a protocol for multiplexed in-situ hybridization (ISH) of the mouse jugular-nodose ganglia complex using RNAscope technology. This enables visualization of gene expression in whole-mounted tissues (ganglia in this case) with low background levels. The authors use Phox2b and Prdm12 to mark neurons located in the nodose vs those in the jugular ganglia and focus on gene transcripts for the GPCRs Cck1r and Ghsr. The protocol is sufficiently detailed and follows up on prior published work by author L Gautron on GPCRs on these vagal sensory affferents.

Major Concerns:

Introduction -- to make their protocol more broadly applicable, I ask that they expand the discussion of vagal ganglia to more species, including pig and human. There is more recent IHC work (Settell 2020 J Neural Eng) and others that highlight distinctions between animals for these ganglia. This is a good point. The proposed changes are included in the revised text.

It is very difficult to see the yellow color in all the Figures, esp in Fig 3. This is even worse in the print versions. It would be beneficial if they used an alternative color when possible, e.g. green, magenta, or cyan. We agree that the yellow RNAScope signals are difficult to see, mostly because the Ghsr mRNA is relatively sparse. We were not able to find a better combination of colors and decided to uniformly and selectively boost the lightness and saturation of the yellow. This is now explained in our figure legends.

Minor Concerns:

It seems that the authors use the term "vagal afferents" to refer to both afferent fibers and afferent cell bodies, which can be confusing. If the authors are referring specifically to nodose ganglia neurons/cell bodies, then they should clarify it as "vagal afferent neurons" which is what this protocol is focused on.

To me, the "afferents" are the actual vagus nerve fibers/axons that innervate the viscera. This is a good point. The proposed changes are included in the revised text.